APPLICATIONS OF
MODELLING AND SIMULATION
http://arqiipubl.com/ams eISSN 2600-8084 VOL 8, 2024, 261-271

Modelling, Simulation and Validation for a Multimode Double-Pendulum Overhead Crane

Sharifah Yuslinda Syed Hussien[1], Hazriq Izzuan Jaafar[1,2*], Rozaimi Ghazali[1,2], Mariam Md Ghazaly[1,2], Mohd Khairul Azizat Johari[3] and Liyana Ramli[4]

[1]Faculty of Electrical Technology and Engineering, Universiti Teknikal Malaysia Melaka, Hang Tuah Jaya, 76100 Durian Tunggal, Melaka, Malaysia
[2]Center for Robotics and Industrial Automation, Universiti Teknikal Malaysia Melaka, Hang Tuah Jaya, 76100 Durian Tunggal, Melaka, Malaysia
[3]Facility Development Department, Johor Port Berhad, 81707 Pasir Gudang, Johor, Malaysia
[4]Faculty of Engineering and Built Environment, Universiti Sains Islam Malaysia, 71800 Nilai, Negeri Sembilan, Malaysia

*Corresponding author: hazriq@utem.edu.my

Submitted 31 May 2024, Revised 13 August 2024, Accepted 02 September 2024, Available online 20 October 2024.

Abstract: This paper focuses on the modelling of a multimode double-pendulum overhead crane (MDPOC) system which generates double-pendulum phenomenon. The MDPOC is far more complex than those of single-pendulum overhead cranes due to the additional degree of freedom, greater nonlinearities, and stronger internal couplings especially involving two or more oscillation frequencies with multimode dynamic effects. More interestingly, two scenarios under fixed and varying cable lengths (payload hoisting) are considered which are closer to the real practical crane. The dynamic crane models are derived using Lagrange's method. Simulations using the Matlab/Simulink block diagram, as well as experiments on a laboratory overhead crane are used to verify and validate the accuracy of MDPOC mathematical modelling. The simulation and experimental results demonstrate the superiority and similar pattern of the trolley position, hook oscillation and payload oscillation under fixed and varying cable lengths that verified the mathematical modelling of MDPOC. It is beneficial for crane operators to understand the dynamic model of MDPOC and useful for future analysis of controller implementation with confidence by researchers.

Keywords: Double-pendulum; Lagrange's method; Overhead crane; Payload hoisting; System modelling.

1. INTRODUCTION

In real-world industrial applications, dynamic modelling is crucial to be explored especially for robotics and control system design [1-2]. By exploring the various techniques of dynamic modelling, a set of mathematical equations can be formulated to represent the actual dynamic behavior of respective systems [3-4]. Interestingly, the system's behavior can be predicted and helps in finding the best potential future outcomes based on the observed data, relationships, and its current state [5-7]. In fact, mathematical modelling enables engineers, designers, or researchers to extract as much information as possible about the particular system under respective conditions without having to practically build the real system, which can be very expensive and dangerous. Since crane system is one of the complex systems and widely used around the world, crane dynamics system is chosen as a suitable industrial application for this study [8].

Cranes are very useful transporters for moving large payloads or dangerous goods from one place to another [9-11]. Accurate positioning with minimal payload oscillation is preferred in the context of industrial cranes transportation to ensure the safe and effective functioning, which can immediately increase industrial production [12-14]. Unfortunately, the rapid motion of the crane is prone to excessive payload oscillation, which may have an impact on placement precision, effectiveness, quality, and safety [15-16]. Since the payload is likely to swing freely and behaves like a pendulum [6], the crane must be operated by highly competent crane operators to operate and minimize the payload's oscillation motions. In that scenario, the crane operator may need to reduce their speed and make appropriate adjustments for the crane's movements to reduce the payload oscillation, which could affect the crane's operation. Therefore, the operation must be paused until the swinging stops.

Most of the literature on cranes treats crane systems as a single pendulum and makes certain assumptions, including without accounting for a hook or an extra sling cable. In addition, the hook and payload are essentially combined and treated as a single mass point to reduce the complexity of the crane model [8,17-18]. These kinds of assumptions may have an impact on the actual behavior of dynamic crane. In fact, double-pendulum cranes with a hook, a payload, and a sling cable are employed in real-world situations. The hook mass is typically used in practical applications and bigger than payload mass [19].

Moreover, the first cable length (between trolley and hook) is longer than the second cable length (between hook and payload), also known as a sling cable. It is because the first cable length can be varied (varying cable length) during payload hoisting [20-24]. In these circumstances, the hook and the payload cause greater oscillations in various frequency modes, resulting in multimode dynamic effects. Multimode is defined as the different oscillation modes between the hook and the payload that generate the phenomenon of two pendulums, known as multimode double-pendulum overhead crane (MDPOC) during transportation.

The MDPOC consists of four outputs (trolley position, hook oscillation angle, payload oscillation angle, and hoisting position) from two input signals (trolley and hoisting forces). On top of that, the MDPOC dynamics are far more complex than those of a single-pendulum crane because of the additional degree of freedom, greater nonlinearities, and stronger internal couplings [25-27]. In other words, good handling of trolley movement is required to achieve hook and payload oscillation suppressions [12]. This is noticeably much more difficult to suppress both oscillations, even for experienced crane operators.

The most popular modelling technique for overhead cranes is the Lagrange's method [8,28-29]. Lagrange's method is a valuable tool in mathematical approach and able to solve complex problems with constraints in various practical scenarios. It simplifies the mathematical process and reduces the number of equations to be solved, primarily due to their effectiveness and simplicity. The Lagrange's method involves with both kinetic energy and potential energy of the crane system to derive motion equations that represent the dynamic model of MDPOC system [30-33]. In this study, two scenarios of a MDPOC that involved fixed and varying cable lengths are considered, which are closer to the real practical crane. Simulations and experiments using a dynamic model and a laboratory MDPOC were conducted, respectively to verify the accuracy of the mathematical modelling. Trolley position, hook oscillation, payload oscillation, and payload hoisting are analyzed, and these are used to study the dynamic model of the MDPOC system. The main contributions of this work are as follows:

1) Dynamic models of a MDPOC that involved a fixed cable length, and a varying cable length (payload hoisting) have been derived. The derived models have been executed via simulation and validated using a laboratory MDPOC.
2) This paper evaluates the effect of hook and payload oscillation frequencies during varying cable length (payload hoisting). This knowledge is important and beneficial for crane operators to understand the dynamic model of MDPOC and can be used for future analysis of controller implementation with confidence by researchers.

2. MATHEMATICAL MODELLING

The dynamic equations for a MDPOC with fixed and variable cable lengths (payload hoisting) are given as provided in Sections 2.1 and 2.2, respectively.

2.1 Fixed Cable Length

In this section, a fixed cable length is studied for the MDPOC as illustrated in Figure 1, where the MDPOC consists of three independent generalized coordinates (trolley position, x, hook angle, θ_1, and payload angle, θ_2). The trolley mass, the hook mass, the payload mass, the fixed cable length, the sling cable, the trolley viscous damping coefficient and the gravitational acceleration constant, represent m, m_1, m_2, l_1, l_2, f_x and g, respectively. F_x is an external trolley force that is applied directly to the MDPOC as the only input signal.

Equation (1) is the Lagrangian equation with respect to the generalized coordinate, q_i, where L represent the Lagrangian function. In addition, T_i and q_i (i =1, 2, 3) represent a non-conservative force and generalized coordinates (q_1, q_2 and q_3 represent x, θ_1 and θ_2), respectively.

$$\frac{d}{dt}\left(\frac{\partial L}{\partial \dot{q}_i}\right) - \frac{\partial L}{\partial q_i} = T_i \tag{1}$$

In addition, the L can be written as Equation (2) where K is the kinetic energy and P is the potential energy.

$$L = K - P \tag{2}$$

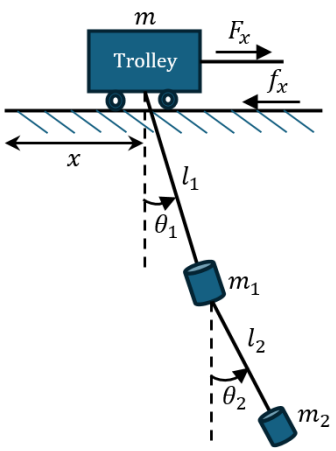

Figure 1. Illustration of MDPOC with a fixed cable length.

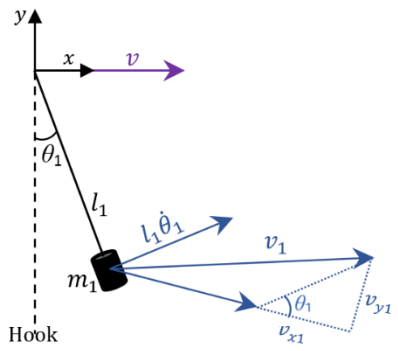

Figure 2. Velocity of hook vector.

Therefore, total K of the MDPOC can be obtained by summing up the trolley kinetic energy, K_x, hook kinetic energy, K_{θ_1} and payload kinetic energy, K_{θ_2} as in Equation (3):

$$K = K_x + K_{\theta_1} + K_{\theta_2} \tag{3}$$

where:

$$K_x = \frac{1}{2}mv^2 \tag{4}$$

$$K_{\theta_1} = \frac{1}{2}m_1{v_1}^2 \tag{5}$$

$$K_{\theta_2} = \frac{1}{2}m_2{v_2}^2 \tag{6}$$

The v, v_1 and v_2 vectors indicate the trolley velocity, hook velocity and payload velocity, respectively:

$$v = \dot{x} \tag{7}$$

$${v_1}^2 = (v + v_{x1})^2 + {v_{y1}}^2 \tag{8}$$

$${v_2}^2 = (v + v_{x1} + v_{x2})^2 + \left(v_{y1} + v_{y2}\right)^2 \tag{9}$$

where v_{x1}, v_{y1}, v_{x2} and v_{y2} can be obtained by using the Pythagoras theorem that yield $v_{x1} = l_1\dot{\theta}_1\cos\theta_1$, $v_{y1} = l_1\dot{\theta}_1\sin\theta_1$, $v_{x2} = l_2\dot{\theta}_2\cos\theta_2$ and $v_{y2} = l_2\dot{\theta}_2\sin\theta_2$. All the respective vectors can be illustrated as in Figures 2 and 3.

By solving Equations (4)-(9) and substituting into Equation (3), the complete K of the MDPOC can be obtained as:

$$\begin{gathered} K = \frac{1}{2}m\dot{x}^2 + \frac{1}{2}m_1\left(\dot{x}^2 + 2\dot{x}l_1\dot{\theta}_1\cos\theta_1 + {l_1}^2{\dot{\theta}_1}^2\right) + \\ \frac{1}{2}m_2\begin{pmatrix}\dot{x}^2 + 2\dot{x}l_1\dot{\theta}_1\cos\theta_1 + 2\dot{x}l_2\dot{\theta}_2\cos\theta_2 + {l_1}^2{\dot{\theta}_1}^2 + {l_2}^2{\dot{\theta}_2}^2 \\ +2l_1l_2\dot{\theta}_1\dot{\theta}_2\cos(\theta_1 - \theta_2)\end{pmatrix} \end{gathered} \tag{10}$$

Furthermore, the total P is only exhibited by the hook (P_{θ_1}) and payload (P_{θ_2}) whereas the trolley potential energy is kept unchanged ($P_x = 0$). Thus, the total P in Figure 4 can be arranged as in Equation (11):

$$P = P_{\theta_1} + P_{\theta_2} \tag{11}$$

where:

$$P_{\theta_1} = m_1gh_1 \tag{12}$$

$$P_{\theta_2} = m_2g(h_1 + h_2) \tag{13}$$

Similarly, h_1 and h_2 can be obtained by using the Pythagoras theorem that yield $h_1 = l_1(1 - \cos\theta_1)$ and $h_2 = l_2(1 - \cos\theta_2)$. Thus, the complete P of the MDPOC can be obtained as:

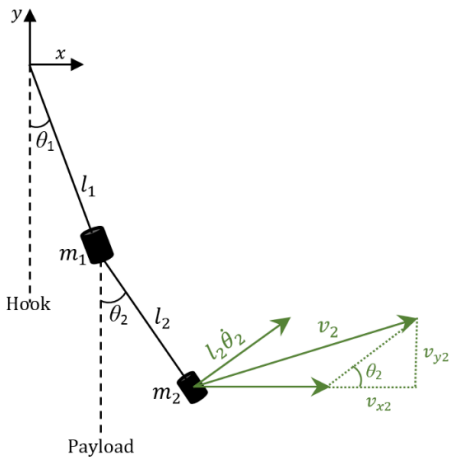

Figure 3. Velocity of payload vector.

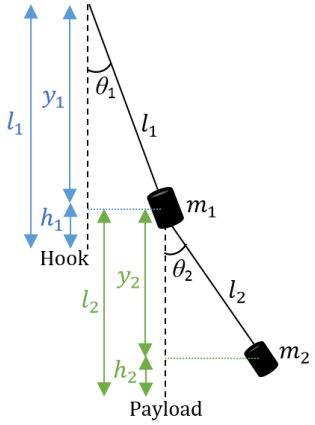

Figure 4. Hook and payload potential energies.

$$P = m_1 g\big(l_1(1-\cos\theta_1)\big) + m_2 g\big(l_1(1-\cos\theta_1) + l_2(1-\cos\theta_2)\big) \tag{14}$$

Therefore, a complete L in Equation (2) can be written as:

$$\begin{aligned} L_{fixed} = {} & \frac{1}{2}m\dot{x}^2 + \frac{1}{2}m_1\left(\dot{x}^2 + 2\dot{x}l_1\dot{\theta}_1\cos\theta_1 + {l_1}^2{\dot{\theta}_1}^2\right) + \\ & \frac{1}{2}m_2\begin{pmatrix}\dot{x}^2 + 2\dot{x}l_1\dot{\theta}_1\cos\theta_1 + 2\dot{x}l_2\dot{\theta}_2\cos\theta_2 + {l_1}^2{\dot{\theta}_1}^2 + {l_2}^2{\dot{\theta}_2}^2 \\ +2l_1l_2\dot{\theta}_1\dot{\theta}_2\cos(\theta_1-\theta_2)\end{pmatrix} - \\ & m_1 g\big(l_1(1-\cos\theta_1)\big) - m_2 g\big(l_1(1-\cos\theta_1) + l_2(1-\cos\theta_2)\big) \end{aligned} \tag{15}$$

By differentiating Equation (15) and obtaining terms as in Equation (1), the dynamic model of MDPOC system with F_x and f_x can be obtained as in Equations (16)-(18) where all the outputs are coupled and highly nonlinear.

$$\begin{aligned} & (m+m_1+m_2)\ddot{x} + (m_1+m_2)l_1\ddot{\theta}_1\cos\theta_1 + m_2l_2\ddot{\theta}_2\cos\theta_2 \\ & -(m_1+m_2)l_1{\dot{\theta}_1}^2\sin\theta_1 - m_2l_2{\dot{\theta}_2}^2\sin\theta_2 = F_x - f_x\dot{x} \end{aligned} \tag{16}$$

$$\begin{aligned} & (m_1+m_2)l_1\ddot{x}\cos\theta_1 + (m_1+m_2){l_1}^2\ddot{\theta}_1 + m_2l_1l_2\ddot{\theta}_2\cos(\theta_1-\theta_2) \\ & + m_2l_1l_2{\dot{\theta}_2}^2\sin(\theta_1-\theta_2) + (m_1+m_2)gl_1\sin\theta_1 = 0 \end{aligned} \tag{17}$$

$$\begin{aligned} & m_2l_2\ddot{x}\cos\theta_2 + m_2l_1l_2\ddot{\theta}_1\cos(\theta_1-\theta_2) + m_2{l_2}^2\ddot{\theta}_2 \\ & - m_2l_1l_2{\dot{\theta}_1}^2\sin(\theta_1-\theta_2) + m_2gl_2\sin\theta_2 = 0 \end{aligned} \tag{18}$$

The nonlinearities (such as sin, cos, or even higher degree of variables) are considered to ensure that the dynamic model agrees with the laboratory MDPOC.

2.2 Varying Cable Length (Payload Hoisting)

In industrial practice, the l_1 changes during payload hoisting, which involves lifting a payload up or down and transfer it at a specific location, as seen in Figure 5. Therefore, F_l is needed as an external hoisting force signal for varying cable length and f_l denotes the viscous damping coefficients of l_1.

By considering the varying cable length, four independent generalized coordinates are obtained by adding an extra independent generalized coordinate that representing l_1 into Equation (1) and accounting for the variable cable length. For that reason, the MDPOC's total kinetic energy is updated with the additional hoisting kinetic energy, K_l which is formulated in Equation (19):

$$K = K_x + K_{\theta_1} + K_{\theta_2} + K_l \tag{19}$$

where K_x is constantly similar with the previous Equations (4) and (7), and K_l can be formulated as:

$$K_l = \frac{1}{2}m_3{v_3}^2 \tag{20}$$

where $v_3 = \dot{l}_1$. Therefore, $K_l = 0$ due to the cable is assumed to be massless ($m_3 = 0$). Nevertheless, the existence of $\dot{l}_1$ provides new $v_{x3} = \dot{l}_1\sin\theta_1$ and $v_{y3} = -\dot{l}_1\cos\theta_1$ as shown in Figure 6.

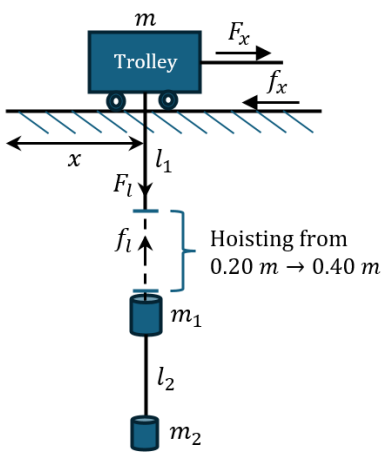

Figure 5. Illustration of MDPOC with a varying cable length (payload hoisting).

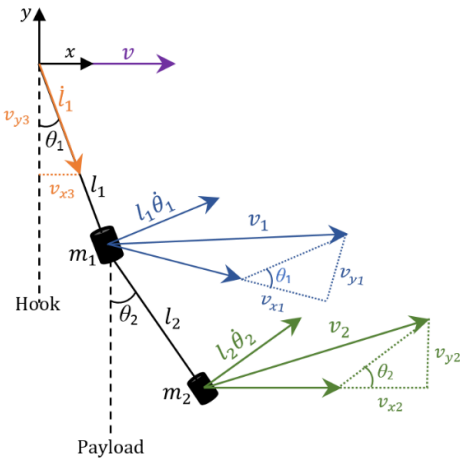

Figure 6. Velocity of hook and payload vectors with a varying cable length.

Thus, the new vectors of v_1 and v_2 can be obtained as:

$$v_1{}^2 = (v + v_{x1} + v_{x3})^2 + (v_{y1} + v_{y3})^2 \tag{21}$$

$$v_2{}^2 = (v + v_{x1} + v_{x2} + v_{x3})^2 + (v_{y1} + v_{y2} + v_{y3})^2 \tag{22}$$

By substituting Equations (21) and (22) into Equations (5) and (6) respectively, the new K_{θ_1} and K_{θ_2} can be formulated as:

$$K_{\theta_1} = \frac{1}{2} m_1 \left(\dot{x}^2 + 2\dot{x} l_1 \dot{\theta}_1 \cos\theta_1 + 2\dot{x}\dot{l}_1 \sin\theta_1 + l_1{}^2 \dot{\theta}_1{}^2 + \dot{l}_1{}^2 \right) \tag{23}$$

$$\begin{aligned} K_{\theta_2} = \frac{1}{2} m_2 (\dot{x}^2 + 2\dot{x} l_1 \dot{\theta}_1 \cos\theta_1 + 2\dot{x} l_2 \dot{\theta}_2 \cos\theta_2 + 2\dot{x}\dot{l}_1 \sin\theta_1 + \\ 2 l_1 l_2 \dot{\theta}_1 \dot{\theta}_2 \cos(\theta_1 - \theta_2) + 2\dot{l}_1 l_2 \dot{\theta}_2 \sin(\theta_1 - \theta_2) + l_1{}^2 \dot{\theta}_1{}^2 + l_2{}^2 \dot{\theta}_2{}^2 + \dot{l}_1{}^2) \end{aligned} \tag{24}$$

Since the P_x and P_l are kept unchanged, the similar P can be obtained as stated in Equation (14). Therefore, the new Lagrangian function can be expressed as in Equation (25).

$$\begin{aligned} L_{hoist} = \frac{1}{2} m \dot{x}^2 + \frac{1}{2} m_1 \left(\dot{x}^2 + 2\dot{x} l_1 \dot{\theta}_1 \cos\theta_1 + 2\dot{x}\dot{l}_1 \sin\theta_1 + l_1{}^2 \dot{\theta}_1{}^2 + \dot{l}_1{}^2 \right) + \\ \frac{1}{2} m_2 (\dot{x}^2 + 2\dot{x} l_1 \dot{\theta}_1 \cos\theta_1 + 2\dot{x} l_2 \dot{\theta}_2 \cos\theta_2 + 2\dot{x}\dot{l}_1 \sin\theta_1 + 2 l_1 l_2 \dot{\theta}_1 \dot{\theta}_2 \cos(\theta_1 - \theta_2) + \\ 2\dot{l}_1 l_2 \dot{\theta}_2 \sin(\theta_1 - \theta_2) + l_1{}^2 \dot{\theta}_1{}^2 + l_2{}^2 \dot{\theta}_2{}^2 + \dot{l}_1{}^2) - \\ m_1 g\big(l_1(1 - \cos\theta_1)\big) - m_2 g\big(l_1(1 - \cos\theta_1) + l_2(1 - \cos\theta_2)\big) \end{aligned} \tag{25}$$

By differentiating Equation (25) based on Equation (1), the dynamic MDPOC model with a varying cable length can be formulated as in Equations (26)-(29).

$$\begin{aligned} (m + m_1 + m_2)\ddot{x} + (m_1 + m_2)(2\dot{l}_1 \dot{\theta}_1 \cos\theta_1 + l_1 \ddot{\theta}_1 \cos\theta_1 - \\ l_1 \dot{\theta}_1{}^2 \sin\theta_1 + \ddot{l}_1 \sin\theta_1) + m_2 l_2 (\ddot{\theta}_2 \cos\theta_2 - \dot{\theta}_2{}^2 \sin\theta_2) = F_x - f_x \dot{x} \end{aligned} \tag{26}$$

$$\begin{aligned} (m_1 + m_2)(\ddot{x} l_1 \cos\theta_1 + l_1{}^2 \ddot{\theta}_1 + g l_1 \sin\theta_1 + 2 l_1 \dot{l}_1 \dot{\theta}_1) + \\ m_2 l_1 l_2 (\ddot{\theta}_2 \cos(\theta_1 - \theta_2) + \dot{\theta}_2{}^2 \sin(\theta_1 - \theta_2)) = 0 \end{aligned} \tag{27}$$

$$\begin{aligned} m_2 l_2 (\ddot{x} \cos\theta_2 + l_2 \ddot{\theta}_2 + \ddot{l}_1 \sin(\theta_1 - \theta_2) - l_1 \dot{\theta}_1{}^2 \sin(\theta_1 - \theta_2) + \\ l_1 \ddot{\theta}_1 \cos(\theta_1 - \theta_2) + 2\dot{l}_1 \dot{\theta}_1 \cos(\theta_1 - \theta_2) + g \sin\theta_2) = 0 \end{aligned} \tag{28}$$

$$\begin{aligned} (m_1 + m_2)\left(\ddot{x} \sin\theta_1 + \ddot{l}_1 - l_1 \dot{\theta}_1{}^2 + g(1 - \cos\theta_1)\right) + \\ m_2 l_2 (\ddot{\theta}_2 \sin(\theta_1 - \theta_2) - \dot{\theta}_2{}^2 \cos(\theta_1 - \theta_2)) = F_l - f_l \dot{l}_1 \end{aligned} \tag{29}$$

3. SIMULATIONS AND EXPERIMENTS SETUP

This section presents the dynamic characteristics of the MDPOC and evaluates the accuracy of the dynamic equations. The derived MDPOC dynamic models with a fixed cable length and a varying cable length were used for simulation, while experiments were carried out on a laboratory MDPOC. Fixed cable length refers to the manually setting of length l_1 by the operator. In this situation, the l_1 is fixed to 0.3 m during transportation. For varying cable length (payload hoisting), it refers to the continuously varying of l_1 from 0.2 m to 0.4 m during payload transportation simultaneously. Figure 7 shows a general block diagram for the simulation and experimental implementation of the MDPOC system.

3.1 Simulations

The dynamic equations presented in Equations (16)-(18) and (26)-(29) were simulated using Matlab/Simulink. Figures 8 and 9 illustrate the Simulink block diagrams for the purpose of solving the dynamic equations and obtaining the trolley motion, hook oscillation angle, payload oscillation angle and payload hoisting for the MDPOC system. The system parameters used in the simulations are listed in Table 1. In this work, the *fcn* block was utilized and run with the solver of ode45 (Dormand-Prince) with a sampling time of 0.001 s.

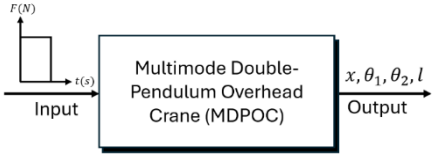

Figure 7. A general block diagram of MDPOC.

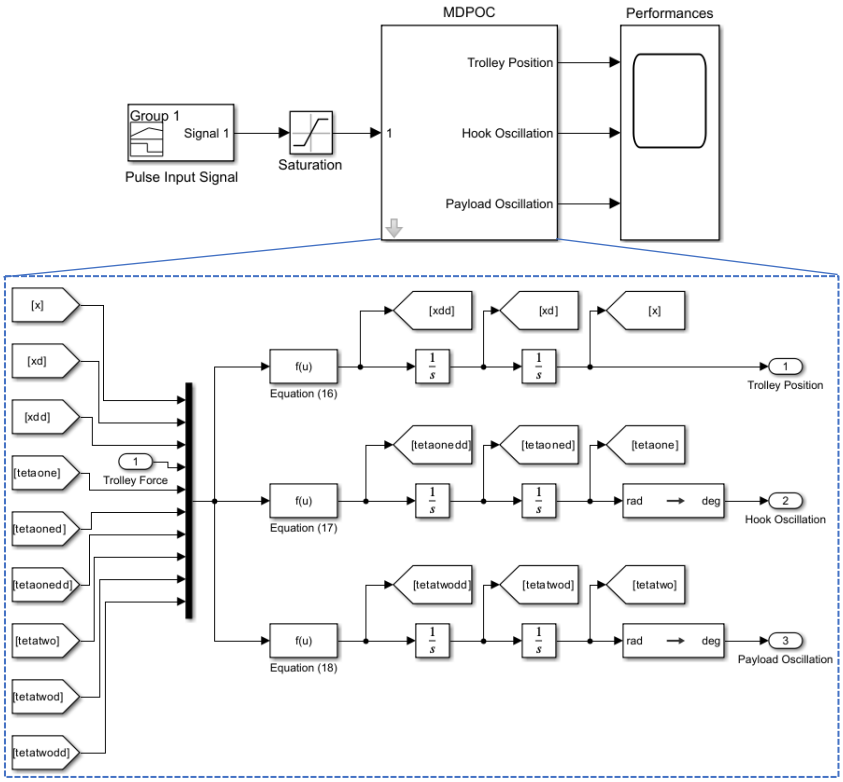

Figure 8. Simulink block of MDPOC.

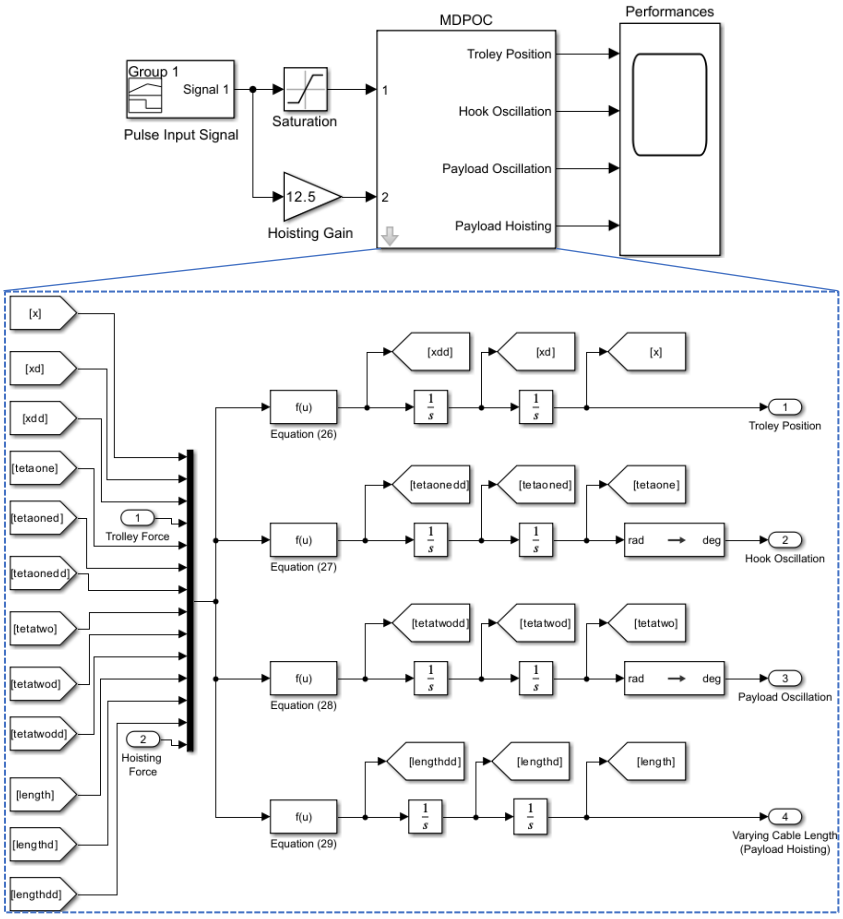

Figure 9. Simulink block of MDPOC with a varying cable length (payload hoisting).

Table 1. MDPOC parameters.

Variables	Parameters	
	Symbol	Values
Trolley Mass	m	1.155 kg
Hook Mass	m_1	0.20 kg
Payload Mass	m_2	0.10 kg
Fixed Cable Length and Varying Cable Length	l_1	0.30 m and 0.20 – 0.40 m
Sling Cable	l_2	0.20 m
Viscous Damping Coefficient of Trolley	f_x	82 Ns/m
Viscous Damping Coefficient of Hoisting	f_l	75 Ns/m
Gravitational Constant	g	9.81 m/s^2

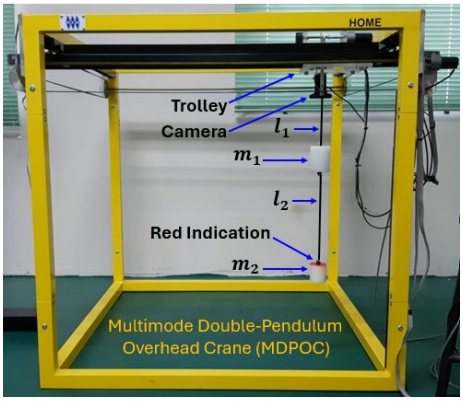

Figure 10. A laboratory MDPOC.

3.2 Experiments

A laboratory overhead crane manufactured by INTECO is transformed as a MDPOC system as shown in Figure 10. This system is fully utilized to verify and validate multimode dynamic models. The crane has a trolley with two cylindrical loads that symbolize the hook and the payload. Three incremental encoders are used to measure the trolley distance, hook oscillation angle, and varying cable length during payload hoisting. In addition, two independent DC motors drive the trolley and hoisting motion systems, respectively. The payload lifting is raised down in a *y*-direction while the trolley is pushed along a rail in *x*-direction as illustrated in Sections 2.1 and 2.2. Furthermore, a trolley-mounted with a Logitech C170 camera angled downward is used to measure the payload oscillation by analyzing the deviation of a red indication located at the top of the payload.

The overhead crane's interface module (RT-DAC board) serves as a communication channel between the computer and the crane. The encoders' measured output signals are supplied to the computer for analysis, after which the computer issues a command to the DC motors. In contrast, the camera is employed to measure the oscillation of the payload and record its movements. Furthermore, executions are implemented in real time using the Matlab/Simulink Real-Time Toolbox. The similar system parameters in Table 1 are used for the experiments, which match the MDPOC employed in the laboratory.

4. RESULTS AND DISCUSSION

All the simulations and experiments were carried out in Matlab/Simulink environment. The responses of the laboratory MDPOC were compared with the simulation results with fixed and varying cable lengths in order to validate the multimode dynamic model. A Simulink block diagram was developed based on Equations (16)-(18) and (26)-(29). Figures 8 and 9 show the Simulink block diagram of the MDPOC system with a fixed cable length and a varying cable length, respectively. An external force (amplitude: 0.6 N and width: 2 seconds) as in Figure 11 was excited into the crane for the trolley movement as illustrated in Figure 12. The simulation and experimental findings of the trolley position, hook oscillation, and payload oscillation are displayed in Figures 12, 13(a) and 13(b), respectively. Interestingly, the patterns of experimental results were consistent with the simulation executions.

Figure 12 illustrates the trolley movement from 0.00 m to 0.40 m within 2.01 seconds (simulation) and 2.18 seconds (experiment). As observed with a fixed cable length, the oscillation responses of the hook and payload were not perfectly in phase. However, the patterns of the oscillations were consistent across both simulations and experiments. Specifically, the maximum payload oscillation angles were recorded as 12.295 degrees in the simulation and 12.250 degrees in the experiment. The oscillation frequencies were 4.490 rad/s in the simulation and 4.621 rad/s in the experiment. These findings are encapsulated in Table 2 with complete details of the maximum oscillations and oscillation frequencies for both the hook and payload oscillation responses. A comparison of these executions reveals a close correlation between the simulated and experimental data, with a maximum relative error of just 3.20% which can be considered small and within an acceptable range. This close agreement underscores the reliability of the simulation model in predicting the dynamic behavior of the MDPOC under the specified conditions.

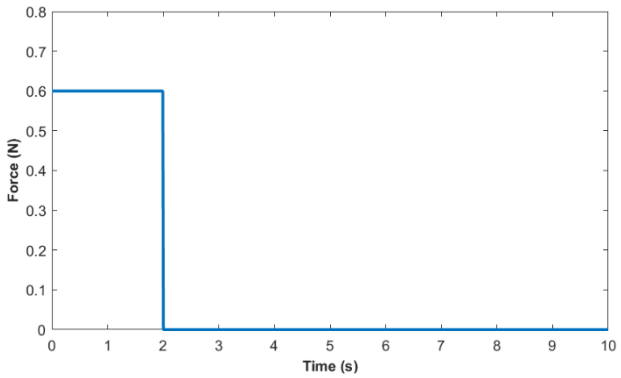

Figure 11. An external trolley force signal.

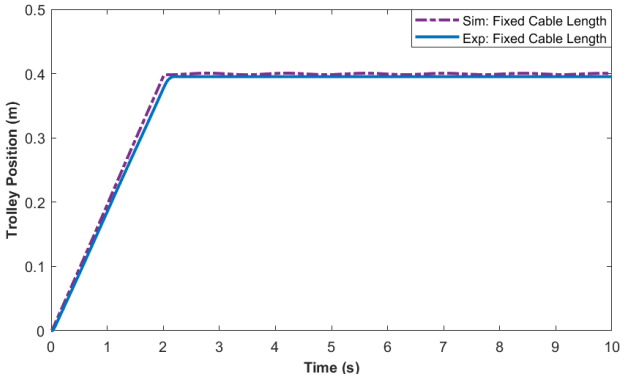

Figure 12. Response of trolley position with a fixed cable length.

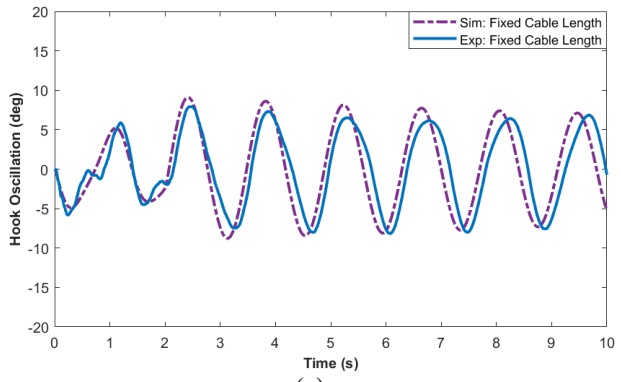

(a)

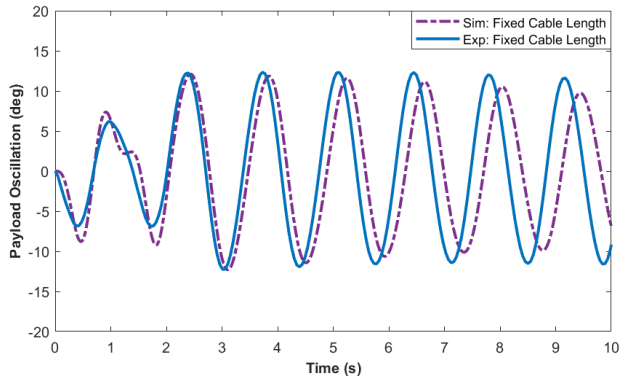

(b)

Figure 13. Response of oscillation with a fixed cable length (a) Hook (b) Payload.

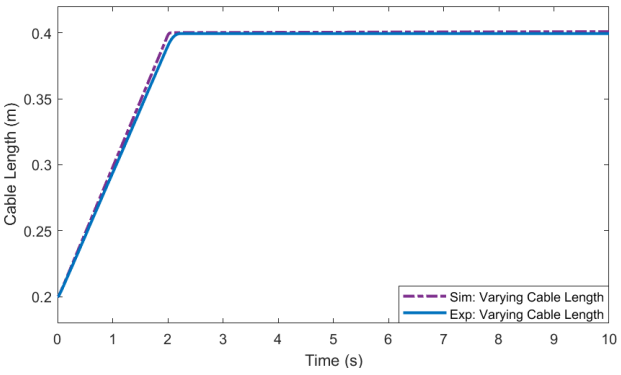

Figure 14. Response of varying cable lengths during payload hoisting.

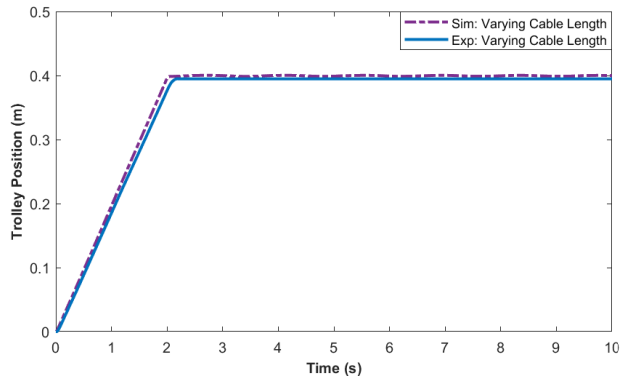

Figure 15. Response of trolley position with a varying cable length.

Table 2. Performance measurement under fixed cable length.

Variables	Max Oscillation		Frequency	
	Hook	Payload	Hook	Payload
Simulation	8.444	12.295	4.477 rad/s	4.490 rad/s
Experiment	8.174	12.250	4.406 rad/s	4.621 rad/s
Relative Error (%)	3.2	0.4	1.6	2.9

To assess the impact of varying cable length (payload hoisting) on the dynamics of a MDPOC, a similar test of simulations and experiments were performed. A similar force signal in Figure 11 was also applied for the payload hoisting operation and excited into the crane system with the hoisting gain of 12.5 as simulated in Figure 9. This simulations and experiments test involved simultaneous trolley motion, hook and payload hoisting, constrained by the laboratory crane's capabilities to a hoisting range from 0.20 m to 0.40 m. Figure 14 shows the response of varying cable length from 0.20 m to 0.40 m during payload hoisting. It was observed that the payload arrived at the destination in 2.09 seconds for simulation and 2.24 seconds for experiment. Figures 15, 16(a) and 16(b) illustrate the oscillation responses of the varying cable length, trolley position, hook and payload oscillation of the MDPOC for both the simulated and experimental scenarios.

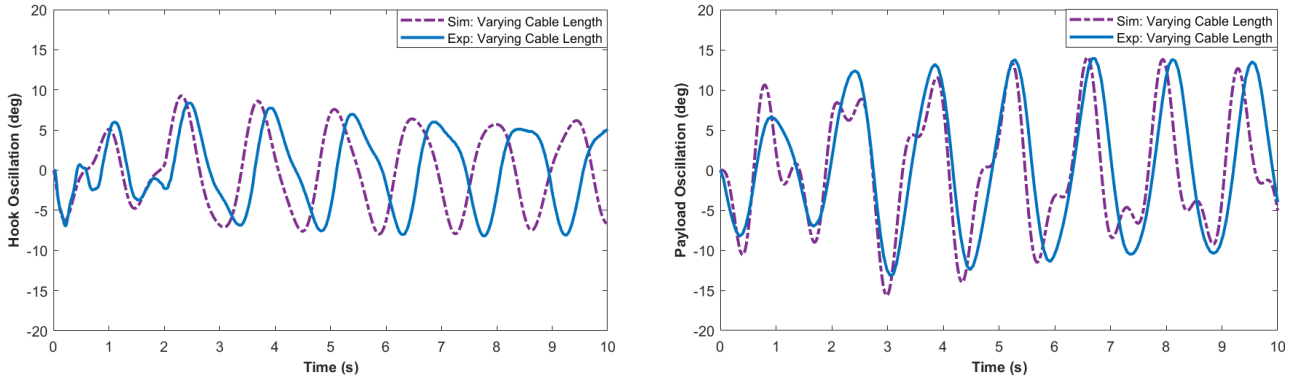

(a) (b)

Figure 16. Response of oscillation with varying cable length (a) Hook (b) Payload.

Table 3. Performance measurement under varying cable length.

Variables	Max Oscillation		Frequency	
	Hook	Payload	Hook	Payload
Simulation	8.602	14.044	9.173 rad/s	8.941 rad/s
Experiment	8.438	13.900	9.299 rad/s	8.665 rad/s
Relative Error (%)	1.9	1.1	1.4	3.1

The analysis of the effects of varying cable length (payload hoisting) on the dynamics of the MDPOC was also conducted based on the oscillation responses as shown in Figure 16. The study revealed that varying the cable length during simultaneous trolley motion significantly impacts the oscillation behavior in terms of maximum hook/payload oscillations and frequencies. Both simulation and experimental results demonstrated similar effects on MDPOC dynamics. During the hoisting operation, specific changes in the maximum hook/payload oscillations were observed. In the simulations, the maximum oscillation value for the hook and payload increased by 1.9% and 14.2%, respectively. The experimental results exhibited a comparable trend, with 3.2% and 13.5% increase for the hook and for the payload, respectively. These findings are recorded in Table 3. As a result, the percentage errors between the simulation and experiment for the hook and payload were 1.9% and 1.1%, respectively, which is considered small.

In addition, the oscillation frequency of both the hook and the payload also showed an increase due to the hoisting operation. Simulation yielded oscillation frequencies of 9.173 rad/s for the hook and 8.941 rad/s for the payload. Similarly, the experiments indicated 9.299 rad/s and 8.665 rad/s for the hook and payload, respectively. Therefore, increasing the cable length during payload hoisting (lowering) generally results in a two-fold increase in hook and payload oscillation frequencies compared to a fixed cable length situation. This behavior is due to the longer cable length providing a greater pendulum effect.

5. CONCLUSION

The dynamic characteristics of a MDPOC under fixed cable length and varying cable length (payload hoisting) are analyzed in this work. It includes the modelling, simulation, and validation of multimode dynamic effects, which generates double-pendulum phenomenon. The impact of trolley position, hook oscillation, and payload oscillation is also explored in this work. The developed model is simulated and verified using a laboratory crane to verify the mathematical modelling of MDPOC. The results from both simulations and experiments show very good compliance with the theoretical predictions. Minor discrepancies between simulation and experimental results, such as maximum oscillation, hook frequency, payload frequency and percentage relative errors, are likely due to modelling assumptions and factors like air friction and wind disturbance that were not considered. Another important observation, the effect of varying cable length provides a two-fold increase in hook and payload oscillation frequencies compared to the fixed cable length scenario, which brings to safety concerns for crane operators. For future work, the effects of twisting, different hook/payload masses and various shapes of payload will be explored to further validate the accuracy of the models. It is beneficial for crane operators to understand the dynamic model of MDPOC and useful for future analysis of controller implementation with confidence by researchers, which can enhance the control and stability of MDPOC under various operating conditions.

ACKNOWLEDGMENT AND FUNDING

The authors would like to thank the Ministry of Higher Education and Universiti Teknikal Malaysia Melaka (UTeM) for providing financial support under FRGS (FRGS/1/2021/TK0/UTEM/02/1) and Universiti Teknologi Malaysia (UTM) for laboratory facilities.

DECLARATION OF CONFLICTING INTEREST

The authors declare no potential conflicts of interest with respect to the research, authorship, and publication of this article.

REFERENCES

[1] S. Zode, S. Sheshank, S. Challa, A. C. Mahato and J. P. Tripathi, Modelling and motion analysis of an automotive seating track using finite element analysis, *Applications of Modelling and Simulation*, 8, 2024, 40-47.

[2] G. D'Ago, M. Selvaggio, A. Suarez, F. J. Ganan, L. R. Buonocore, M. Di Castro, V. Lippiello, A. Ollero and F. Ruggiero, Modelling and identification methods for simulation of cable-suspended dual-arm robotic systems, *Robotics and Autonomous System*, 175, 2024, 104643.

[3] Y. Zhang, M. Li and C. Yang, Robot learning system based on dynamic movement primitives and neural network, *Neurocomputing*, 451, 2021, 205-214.

[4] K. Katsampiris-Salgado, K. Haninger, C. Gkrizis, N. Dimitropoulos, J. Kruger, G. Michalos and S. Makris, Collision detection for collaborative assembly operations on high-payload robots, *Robotics and Computer-Integrated Manufacturing*, 87, 2024, 102708.

[5] H. I. Jaafar, Z. Mohamed, J. J. Jamian, A. F. Z. Abidin, A. M. Kassim and Z. A. Ghani, Dynamic behaviour of a nonlinear gantry crane system, *Procedia Technology*, 11, 2013, 419-425.

[6] M. R. Mojallizadeh, B. Brogliato and C. Prieur, Modeling and control of overhead cranes: A tutorial overview and perspectives, *Annual Reviews in Control*, 56, 2023, 100877.

[7] M. M. Bello, Z. Mohamed, M. Ö. Efe and H. Ishak, Modelling and dynamic characterisation of a double-pendulum overhead crane carrying a distributed-mass payload, *Simulation Modelling Practice and Theory*, 134, 2024, 102953.

[8] K. H. Umer and H. Shah, *Control Dynamics and Control of Industrial Cranes*, Singapore: Springer, 2019.

[9] E. M. Abdel-Rahman, A. H. Nayfeh and Z. N. Masoud, Dynamics and control of cranes: A review, *Journal of Vibration and Control*, 9, 2003, 863-908.

[10] L. Ramli, Z. Mohamed, A. M. Abdullahi, H. I. Jaafar and I. M. Lazim, Control strategies for crane systems: A comprehensive review, *Mechanical Systems and Signal Processing*, 95, 2017, 1-23.

[11] M. Hussein and T. Zayed, Crane operations and planning in modular integrated construction: Mixed review of literature, *Automation in Construction*, 122, 2021, 103466.

[12] N. Sun, T. Yang, Y. Fang, Y. Wu and H. Chen, Transportation control of double-pendulum cranes with a nonlinear quasi-PID scheme: Design and experiments, *IEEE Transactions on System, Man, and Cybernetics: Systems*, 49, 2019, 1408-1418.

[13] Z. Tian, L. Yu, H. Ouyang and G. Zhang, Transportation and swing reduction for double-pendulum tower cranes using partial enhanced-coupling nonlinear controller with initial saturation, *ISA Transactions*, 112, 2021, 122-136.

[14] H. D. Tho, N. Uchiyama and K. Terashima, Resonance-based tossing control for bulk materials transportation of an overhead crane, *IEEE Transactions on Industrial Electronics*, 68, 2021, 609-621.

[15] S. Sadeghi, N. Soltanmohammadlou and P. Rahnamayiezekavat, A systematic review of scholarly works addressing crane safety requirements, *Safety Science*, 133, 2021, 105002.

[16] S. R. Mohandes, S. Abdelmageed, S. Hem, J. S. Yoo, T. Abhayajeewa and T. Zayed, Occupational health and safety in modular integrated construction projects: The case of crane operations, *Journal of Cleaner Production*, 342, 2022, 130950.

[17] N. Sun, Y. Fang, H. Chen and B. Lu, Amplitude-saturated nonlinear output feedback antiswing control for underactuated cranes with double-pendulum cargo dynamics, *IEEE Transactions on Industrial Electronics*, 64, 2017, 2135-2146.

[18] A. Mohammed, H. Altuwais and K. Alghanim, An optimized shaped command of overhead crane nonlinear system for rest-to-rest maneuver, *Journal of Engineering Research*, 11, 2023, 548-554.

[19] N. Sun, Y. Wu, Y. Fang and H. Chen, Nonlinear antiswing control for crane systems with double-pendulum swing effects and uncertain parameters: Design and experiments, *IEEE Transactions on Automation Science and Engineering*, 15, 2018, 1413-1422.

[20] A. M. Abdullahi, Z. Mohamed, H. Selamat, H. R. Pota, M. S. Zainal Abidin and S. M. Fasih, Efficient control of a 3D overhead crane with simultaneous payload hoisting and wind disturbance: Design, simulation and experiment, *Mechanical Systems and Signal Processing*, 145, 2020, 106893.

[21] M. Li, H. Chen and R. Zhang, An input dead zones considered adaptive fuzzy control approach for double pendulum cranes with variable rope lengths, *IEEE/ASME Transactions on Mechatronics*, 27, 2022, 3385-3396.

[22] M. Li, H. Chen and Z. Li, Input-limited optimal control for overhead cranes with payload hoisting/lowering and double pendulum effects, *Nonlinear Dynamics*, 111, 2023, 11135-11151.

[23] D. Li, T. Xie, G. Li, J. Yao and S. Hu, Adaptive coupling tracking control strategy for double-pendulum bridge crane with load hoisting/lowering, *Nonlinear Dynamics*, 112, 2024, 8261-8280.

[24] S. Wang, W. Jin and W. Chen, A novel payload swing control method based on active disturbance rejection control for 3D overhead crane systems with time-varying rope length, *Journal of the Franklin Institute*, 361, 2024, 106707.

[25] H. Ouyang, B. Zhao and G. Zhang, Enhanced-coupling nonlinear controller design for load swing suppression in three-dimensional overhead cranes with double-pendulum effect, *ISA Transactions*, 115, 2021, 95-107.

[26] H. I. Jaafar, Z. Mohamed, M. A. Ahmad, N. A. Wahab, L. Ramli and M. H. Shaheed, Control of an underactuated double-pendulum overhead crane using improved model reference command shaping: Design, simulation and experiment, *Mechanical Systems and Signal Processing*, 151, 2021, 107358.

[27] S. Arabasi and Z. Masoud, Frequency-modulation input-shaping strategy for double-pendulum overhead cranes undergoing simultaneous hoist and travel maneuvers, *IEEE Access*, 10, 2022, 44954-44963.
[28] D. Qian and J. Yi, *Hierarchical Sliding Mode Control for Under-Actuated Cranes*, Berlin, Heidelberg: Springer, 2015.
[29] A. Talaeizadeh, M. Forootan, M. Zabihi and H. N. Pishkenari, Comparison of kane's and lagrange's methods in analysis of constrained dynamical systems, *Robotica*, 38, 2020, 2138-2150.
[30] M. M. Bello, Z. Mohamed, S. M. F. ur Rehman, W. A. Balogun, K. Aibek and S. Gamzat, Multi-mode input shapers for oscillation control of an overhead crane with distributed mass payload, *Applications of Modelling and Simulation*, 8, 2024, 191-200.
[31] M. Giacomelli, F. Padula, L. Simoni and A. Visioli, Simplified input-output inversion control of a double pendulum overhead crane for residual oscillations reduction, *Mechatronics*, 56, 2018, 37-47.
[32] H. Ouyang, J. Hu, G. Zhang, L. Mei and X. Deng, Sliding-mode-based trajectory tracking and load sway suppression control for double-pendulum overhead cranes, *IEEE Access*, 7, 2019, 4371-4379.
[33] B. Lu, Y. Fang and N. Sun, Enhanced-coupling adaptive control for double-pendulum overhead cranes with payload Hoisting and Lowering, *Automatica*, 101, 2019, 241-251.